Journal of Astronomical Telescopes, Instruments, and Systems

AstronomicalTelescopes.SPIEDigitalLibrary.org

Design of conical Wolter-I geometry with sectioned secondary mirrors for x-ray telescopes

Yingyu Liao
Zhengxiang Shen
Zhanshan Wang

SPIE.

Yingyu Liao, Zhengxiang Shen, Zhanshan Wang, "Design of conical Wolter-I geometry with sectioned secondary mirrors for x-ray telescopes," *J. Astron. Telesc. Instrum. Syst.* **5**(1), 014004 (2019), doi: 10.1117/1.JATIS.5.1.014004.

Design of conical Wolter-I geometry with sectioned secondary mirrors for x-ray telescopes

Yingyu Liao,[a,b] Zhengxiang Shen,[a,b] and Zhanshan Wang[a,b,*]
[a]Ministry of Education, Tongji University, Key Laboratory of Advanced Micro-Structured Materials, Shanghai, China
[b]Tongji University, Institute of Precision Optical Engineering, School of Physics Science and Engineering, Shanghai, China

Abstract. Conical Wolter-I geometry is employed for many x-ray telescopes to lower their cost and fabrication difficulty at the expense of angular resolution. Owing to the conic error, the angular resolution of conical Wolter-I geometry is much worse than that of Wolter-I geometry, especially for the telescopes with large diameter. We optimized the conical Wolter-I geometry to significantly improve the angular resolution. We designed a conical Wolter-I geometry with sectioned secondary mirrors. Based on the normal conical Wolter-I geometry, we divided the secondary mirror into two equal sections along the optical axis. In this case, the collecting area was reduced by 5% because of the interval between the two sections. Meanwhile, the conic error was reduced by about 50%, indicating a great improvement in angular resolution. Regarding our improvement in the thermal slumping technique, it is feasible to fabricate sectioned mirrors, thus improving the angular resolution by 50% at the cost of a 5%-reduction in collecting area. In addition, a hybrid geometry, comprising the sectioned and nonsectioned geometries, is proposed as an alternative for x-ray telescopes with a large amount of nested shells, to obtain both a large collecting area and decent angular resolution. [DOI: 10.1117/1.JATIS.5.1.014004]

Keywords: x-ray telescope; conical Wolter-I geometry; optical design; ray-tracing program.

Paper 18068 received Aug. 23, 2018; accepted for publication Dec. 26, 2018; published online Jan. 25, 2019.

1 Introduction

Throughout the history of x-ray astronomy, grazing-incidence telescopes have played very important roles in x-ray observation, and Wolter-I geometry has been considered very crucial in grazing-incidence x-ray observation. In 1952, Wolter described several variations (types I, II, and III) of the grazing-incidence imaging x-ray optical system.[1] The profile of each type consists of two coaxial and confocal conic section curves, which can approximately satisfy the Abbe sine condition and eliminate on-axis aberration. Subsequently, Wolter formulated completely aplanatic versions of his designs (i.e., Wolter–Schwarzschild designs[2]), which fulfilled the Abbe sine condition exactly and thus eliminated the coma aberration for paraxial rays. A multilayer nested Wolter-I geometry, consisting of pairs of coaxial and nested confocal paraboloid-hyperboloids, was proposed by VanSpeybroeck and Chase[3] in 1972. The nested Wolter-I geometry, characterized by a high resolution and large collecting area, then became the model for high-resolution x-ray telescopes in orbit.

Even though the Wolter-I geometry has a great on-axis performance, the angular resolution degrades rapidly with the off-axis angle. In the case of large fields of view (FOV), to achieve a decent angular resolution over the whole FOV, several different mirror shapes have been proposed based on Wolter-I geometry. According to Werner's design[4] (1977), mirror surfaces described by polynomials (with terms higher than the second-order) have been proposed to improve the performance over the FOV at the cost of the on-axis resolution. The merit function was determined and used to optimize the polynomials for large-field x-ray imaging.[5,6] Harvey and Thompson[7,8] presented the idea of a telescope constructed from two hyperboloid surfaces, which provided a great performance over an FOV of 20′. In addition, a simple sag adjustment of the primary mirrors in the modified Wolter–Schwarzschild telescope can be used to improve the off-axis optical performance.[9] These quadric solutions are well suited for optimization purposes, which can be used to improve the off-axis angular resolution at the cost of the on-axis performance.

Telescopes using Wolter-I geometry include the Apollo Telescope Mount[10] (1973 to 1974), Einstein Observatory[11] (1978 to 1981), EXOSAT[12] (1983 to 1986), ROSAT[13] (1990 to 1999), Chandra X-ray Observatory[14] (1999–), XMM-Newton telescope[15] (1999–), Swift XRT[16] (2004–), and eROSITA telescope[17] (to be launched in 2019). In addition, Wolter–Schwarzschild geometry is employed for the EUVE telescope,[18] whereas hyperboloid–hyperboloid geometry is adopted for the Solar X-ray Imager telescope.[19]

Nevertheless, with the employment of Wolter-I geometry and its optimization solutions, the mirrors are costly and difficult to fabricate. Petre and Serlemitsos[20,21] designed a conical Wolter-I geometry. They approximated the parabola and hyperbola surface of the Wolter-I geometry with double cones. This solution could greatly lower the cost and difficulty of mirror fabrication by compromising the focusing performance. For missions that require a modest resolution but large effective area, it is suitable to adopt the conical Wolter-I geometry with plenty of nested shells. Many telescopes employ the conical Wolter-I geometry, such as ASCA[22] (1993 to 2001), BeppoSAX[23] (1996 to 2002), Suzaku[24] (2005 to 2015), NuSTAR[25] (2012–), and Astro-H[26] (2016).

Compared to Wolter-I geometry and its quadric solutions, conical Wolter-I geometry has significant advantages of lower

*Address all correspondence to Zhanshan Wang, E-mail: wangzs@tongji.edu.cn

cost and easy fabrication. In this case, the collecting area can be enhanced further by additional nested mirror shells. However, because of the conic error, the conical Wolter-I geometry inevitably corresponds to a poor focusing performance, especially regarding the on-axis angular resolution. With the growing demand for more effective observations of deep space, x-ray telescopes with larger effective areas but decent angular resolutions are required. With the development of several mirror fabrication processes, including epoxy replication technology (first applied in EXOSAT mission), thermal slumping technology (currently only applied in NuSTAR mission, first proposed in an experimental KB telescope[27]), and Silicon Pore Optics technology[28–31] (in past XEUS and IXO missions, current ATHENA mission), x-ray telescopes adopting the conical Wolter-I geometry are promisingly achieving unprecedented effective areas by nesting many more mirror shells. Meanwhile, the angular resolution degrades with additional mirror shells (i.e., with an increasing diameter of the telescope) for a given focal length. By shortening the mirror length, we reduce the conic error, thus improving the resolution. However, for a given telescope diameter and mirror thickness, more nested mirrors are required. The collecting area is thereby decreased as a result of more geometric obstructions from extra nested mirrors.

Considering the equilibrium between effective area and angular resolution, as well as the time and money spent on x-ray telescope fabrication, Chen et al.[32] presented three x-ray telescope structures based on Wolter-I geometry, which use one conical surface and one quadric surface as the mirror pair, respectively. Among the three structures, Chen et al. concluded that the geometry consisting of one cone surface and one hyperbola surface (CH structure) was characterized by the best focusing performance. This CH structure was expected to have an improved resolution about 57% better than that of the double-cone structure (i.e., the conical Wolter-I geometry). The CH structure indeed had a greatly improved angular resolution but was quite difficult and costly to fabricate compared to the double-cone structure. However, the fabrication of the quadric surface was still challenging, even with the mirror fabrication of the CH structure being less time-consuming than the double quadric structure (including Wolter-I geometry and its quadric optimization solutions).

To balance the performance and fabrication of the x-ray telescope, we designed a conical Wolter-I geometry with sectioned secondary mirrors. Based on the normal conical Wolter-I geometry, we divided the secondary mirror into two equal sections along the optical axis. Note that the normal rays will still undergo double-reflection rather than triple-reflection. In other words, the normal rays, reflected by the primary mirror, will only strike either of the two secondary sections, and then converge to the focal plane. In this case, the sectioned structure was expected to have an improved resolution about 50% better than that of the normal conical Wolter-I geometry, at the cost of a reduction of about 5% in collecting area. In this paper, the design and simulation of such a kind of geometry are introduced in detail. In addition, a hybrid geometry, consisting of the sectioned and nonsectioned geometries, is introduced as an alternative for x-ray telescopes with a large amount of nested shells.

2 Design of Conical Wolter-I Geometry with Sectioned Secondary Mirrors

The Einstein Probe (EP) mission[33] was proposed in 2012 and is one of the candidate missions for advanced study in the Chinese Academy of Sciences space science program. It will carry a follow-up X-ray Telescope (FXT) with a narrow field of view for observation, employing the conical Wolter-I geometry. The optical design and simulation of the FXT have been introduced in detail in a previous publication.[34]

Figure 1 is a schematic of the EP FXT. In principle, the focal length of the Wolter-I geometry is defined as the axial distance between the focus and the intersection plane of the paraboloid and hyperboloid.[3] Approximately, we define that the nested shells of the FXT share the common focal length, which is the axial length from the focus to the midpoint between the primary and secondary mirrors. In the case of incoming parallel beams, the rays that strike the center of the primary mirrors will be reflected onto the center of the secondary mirrors and then converge to the focus, as demonstrated by the red dashed line in Fig. 1. For the primary mirror and secondary mirror, the nominal grazing angles θ are defined identically, to maximize the on-axis collecting area.

According to the scientific requirement and mirror fabrication process, we have fixed the initial parameters of mirror length L (100 mm), mirror thickness t (0.3 mm), focal length f (2052.5 mm), and interval gap (5 mm). In addition to the given parameters of L, t, f, and gap, the EP FXT is characterized by a set of radii of mirrors with respect to the optical axis, i.e., R_{out}, R_{in}, r_{out}, and r_{in}, as shown in Fig. 1. The parameters of nested shells are calculated shell by shell, from the outside to inside. Taking the outermost mirror shell as an example, the parameters can be determined as follows:

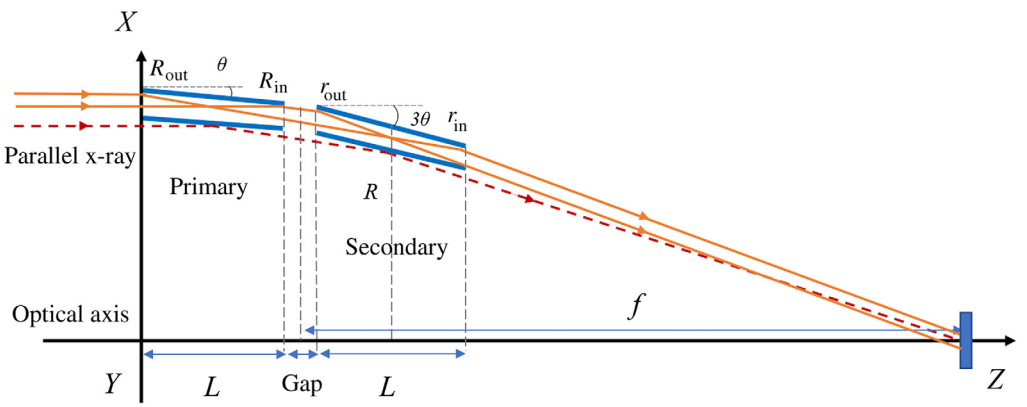

Fig. 1 Schematic of the EP FXT. Shells are nested tightly to maximize the on-axis collecting area.

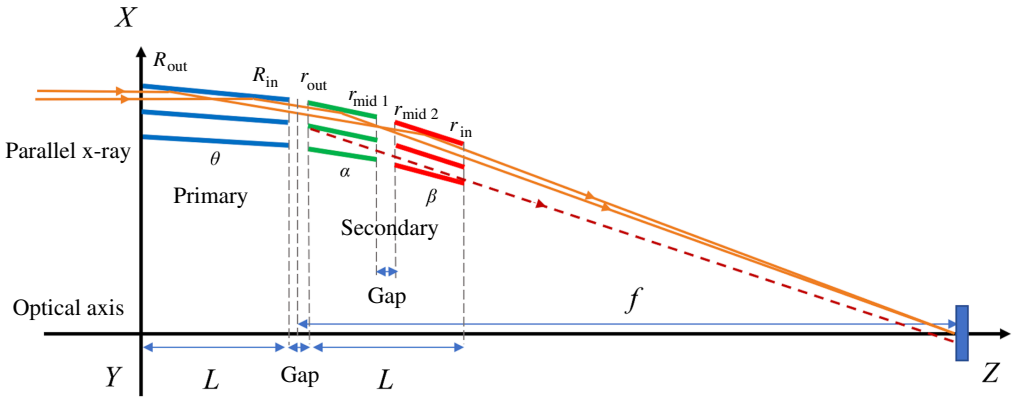

Fig. 2 Schematic of the sectioned FXT, where the parameters are defined similarly to the nonsectioned FXT.

$$\theta = \arctan\left(\frac{R}{f - \frac{L+\text{gap}}{2}}\right)/4, \tag{1}$$

$$R_{\text{out}} = (L + \text{gap}) \times \tan(2\theta) + R + \frac{L}{2} \times \tan(\theta), \tag{2}$$

$$R_{\text{in}} = (L + \text{gap}) \times \tan(2\theta) + R - \frac{L}{2} \times \tan(\theta), \tag{3}$$

$$r_{\text{out}} = R + \frac{L}{2} \times \tan(3\theta), \tag{4}$$

$$r_{\text{in}} = R - \frac{L}{2} \times \tan(3\theta), \tag{5}$$

where R represents the radius of the center of the outermost secondary mirror with respect to the optical axis, which is given as an initial value.

Based on the conical Wolter-I geometry of the EP FXT (hereafter called the nonsectioned FXT), we divide every secondary mirror into two equal sections, the front section (green line, corresponding to the oblique angle α) and rear section (red line, corresponding to the oblique angle β). This geometry (hereafter called the sectioned FXT) is shown in Fig. 2. It should be noted that the normal rays still undergo double-reflection rather than triple-reflection; even the secondary mirrors are divided into two parts. The normal rays, reflected by the primary mirror, will only strike either of the two secondary sections, and they will then converge to the focal plane. In the case of incoming parallel rays, the rays, reflected onto the center of the front section or rear section, will converge to the focus. As a result, the angles between the two sections and optical axis (i.e., oblique angles), α and β, satisfy the inequality $\alpha < 3\theta < \beta$. An increased grazing angle of incidence at the rear section implies a reduction in reflectivity, which is partly compensated by the decreased grazing angle of incidence at the front section. Similarly, to maximize the on-axis collecting area, the shells are nested tightly. A beam path diagram of the nonsectioned and sectioned FXT is shown in Fig. 3. The reduction in collecting area is ascribed to the interval between the two sections of the secondary mirror (~5% reduction for EP FXT, geometrically depending on the mirror length L and the interval gap), while the half

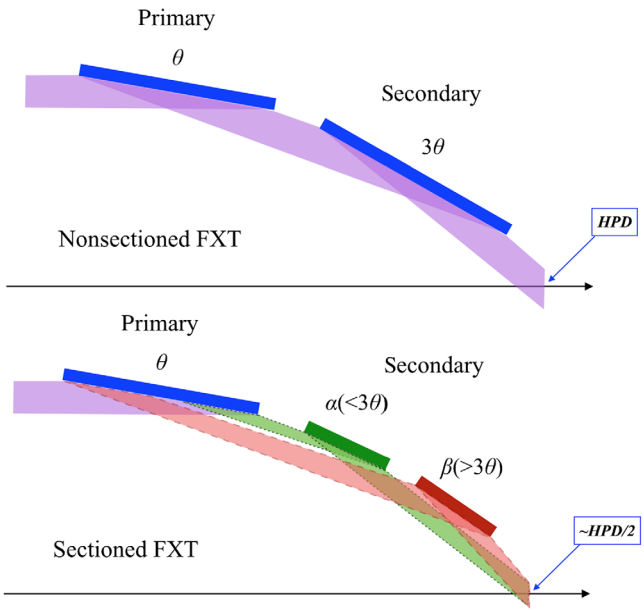

Fig. 3 Beam path of two kinds of geometry, the nonsectioned FXT and sectioned FXT.

power diameter (HPD) improvement (~50%) profits from the sectioned geometry.

The structural parameters of the sectioned FXT are derived from the parameters of the nonsectioned FXT. Apart from the calculated parameters of R_{out}, R_{in}, r_{out}, and r_{in} for the nonsectioned FXT, two more sets of radii are required to characterize the sectioned FXT, i.e., r_{mid1} and r_{mid2}, as shown in Fig. 2. As mentioned above, in the case of incoming parallel rays, those rays that reflect onto the center of the front section or rear section of the secondary mirror will converge to the focus, respectively. Under this constraint, the parameters of r_{mid1} and r_{mid2} are derived from the known parameters of R_{out}, R_{in}, r_{out}, and r_{in}, which are described mathematically via Eqs. (6)–(9).

First, oblique angles of the two sections of the secondary mirror, α and β, can be determined from the following equations:

$$r_{\text{out}} = \left(f - \frac{L + \text{gap}}{4}\right) \times \tan(2\alpha - 2\theta) + \frac{L - \text{gap}}{4} \times \tan(\alpha), \tag{6}$$

$$r_{\text{in}} = \left(f - \frac{3L + 3\text{gap}}{4}\right) \times \tan(2\beta - 2\theta) - \frac{L - \text{gap}}{4} \times \tan(\beta). \tag{7}$$

Next, the parameters of r_{mid1} and r_{mid2} can be calculated as

$$r_{\text{mid1}} = r_{\text{out}} - \frac{L - \text{gap}}{2} \times \tan(\alpha), \tag{8}$$

$$r_{\text{mid2}} = r_{\text{in}} + \frac{L - \text{gap}}{2} \times \tan(\beta). \tag{9}$$

Then, the tightly nested structure implies that the rays reflected by the two sections of secondary mirrors will converge exactly to the focal plane without the obscuration resulting from the inner mirrors, similar to the red dashed line shown in Fig. 2. Hence,

$$r_{\text{in}_{i+1}} = r_{\text{out}_i} - [L \times \tan(2\alpha_i - 2\theta_i) + t], \tag{10}$$

where the subscripts i and $i + 1$ represent the outer shell and inner shell, respectively. Via Eq. (10), the parameters of the rest of the shells are calculated iteratively, shell by shell, and from the outside to inside.

3 Simulation of Conical Wolter-I Geometry with Sectioned Secondary Mirrors

The structural parameters of both the sectioned and nonsectioned FXT were derived mathematically for comparison. The parameters were determined based on the same initial values, including mirror length L (100 mm), mirror thickness t (0.3 mm), focal length f (2052.5 mm), and interval gap (5 mm), as well as the same diameter of aperture from 80 to 250 mm. The main characteristics of the two types of FXT are summarized in Table 1. For comparison, characteristics of the nonsectioned FXT with shorter mirrors ($L = 50$ mm) is shown in Table 1 as well. Being sectioned does not elucidate the difference in basic parameters of the FXT, such as the number of shells N or grazing angle θ. With regard to the basic performance, the HPD of the sectioned FXT significantly improves at the cost of a slight reduction in GA. By contrast, shortening mirror length is less effective than sectioning secondary mirrors. According to Table 1, the angular resolution improved significantly as the sectioned FXT did. Nevertheless, for a given diameter of 80 to 250 mm and mirror thickness of 0.3 mm, much more nested mirrors are required for the nonsectioned FXT with shorter mirrors. The geometric area is inevitably decreased by 17% as a result of more geometric obstructions from extra nested mirrors. The geometric area of the sectioned FXT is only decreased by 5%, which can be smaller by shortening the interval between sectioned secondary mirrors using improved fabrication process.

Simulations using a ray-tracing program have been performed to evaluate the performance of the sectioned FXT. Further investigation of the performance of the sectioned FXT will be introduced, with the simulations of the nonsectioned FXT for comparison ($L = 100$ mm).

3.1 *Effective Area*

In this section, we present the variation in effective area with photon energy and off-axis angle in Fig. 4. A set of coatings was designed to optimize the effective area of the EP FXT, which has been introduced in a previous publication.[34] Compared to the nonsectioned FXT, there is a slight reduction in effective area of the sectioned FXT, about 5%, at a lower energy band of 0.5 to 4 keV. Despite the reduction in effective area, the FOV (30′) of the sectioned FXT basically remains unchanged, and the slight reduction can be compensated by several extra mirrors shells.

3.2 *Angular Resolution*

With respect to the angular resolution (i.e., HPD), the sectioned FXT is superior to the nonsectioned FXT, both on axis and off axis. Except for a great on-axis HPD, the sectioned FXT is

Table 1 Characteristics of the nonsectioned and sectioned FXT.

	Nonsectioned FXT	Sectioned FXT	Nonsectioned FXT (with shorter mirrors)
Mirror length L (mm)	100	Primary mirror 100 secondary mirror 47.5 + 47.5	50
Mirror thickness t (mm)	0.3	0.3	0.3
Focal length f (mm)	2052.5	2052.5	2052.5
Interval gap (mm)	5	5	5
Diameter D (mm)	80 to 250	80 to 250	80 to 250
Number of shells N	66	66	107
Grazing angle θ (deg)	0.29 to 0.89	0.29 to 0.89	0.29 to 0.88
FOV (′)	30	30	30
Angular resolution (HPD) (″)	54.3	25.7	26.9
Geometric area (GA) (cm^2)	300	284	250

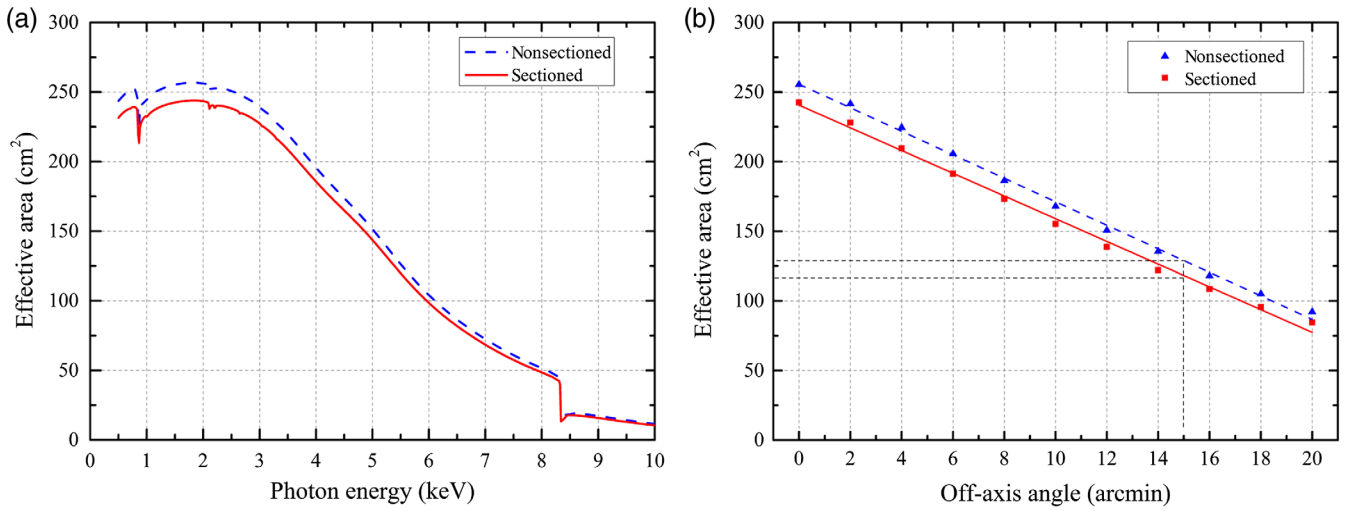

Fig. 4 (a) Variation in on-axis effective area with photon energy of nonsectioned and sectioned FXT. (b) Variation in effective area with off-axis angle at 1.5 keV of nonsectioned and sectioned FXT.

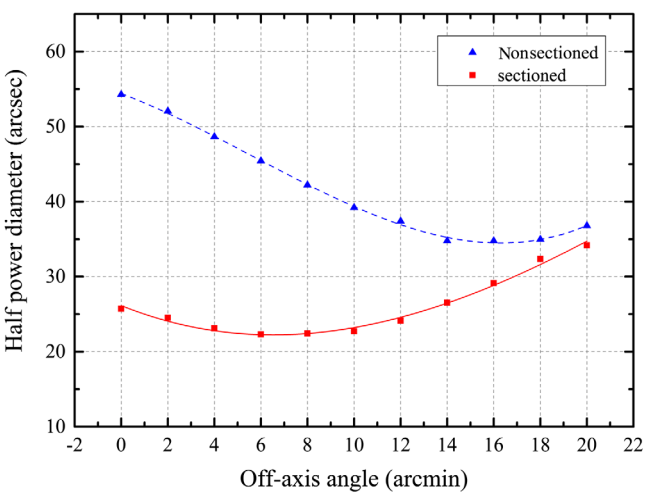

Fig. 5 Variation in HPD with off-axis angle of nonsectioned and sectioned FXT.

characterized by a decent angular resolution over the whole FOV, which is insensitive to the variation in off-axis angle and better than 30″. By contrast, the HPD of the nonsectioned FXT is worse than 34″ and is sensitive to the off-axis angle over the whole FOV. The variation in HPD with off-axis angle is shown in Fig. 5.

3.3 *Stray Light*

Stray light reaches the focal plane without the normal double reflection and creates a ghost image or an additional background in the detector FOV. Consequently, stray light hampers x-ray astronomical observations to some extent. As shown in Table 1, the basic parameters of the nonsectioned and sectioned FXT are considerably consistent, and the behaviors of stray light in these two types of FXT are also consistent. Here, we take the sectioned FXT for example, presenting the investigation of the stray light behavior.

Some rays only undergo a single reflection inside the optic. In other words, they only reflect from either the primary or secondary mirror. These rays are primary (p) stray light and secondary (s) stray light, respectively. Except for p and s stray lights, there are other components of stray light, such as backside stray light and stray light without reflection, which are much fainter than p and s stray lights in brightness, especially for tightly nested geometry. In Fig. 6, the four components of stray light are illustrated.

For nested mirror shells, the spacing of the shells makes it possible for photons to strike the focal plane without normal double reflection. Even though the sectioned FXT has an advantage of reducing stray light benefiting from its tightly nested structure, not all stray light can be eliminated. We simulated the behaviors of stray light in the sectioned FXT using a ray-tracing program. Among the four components of stray light, the backside stray light is not considered, because it requires very high fluxes to be detected and cannot be seen from typical astrophysical sources, except for solar observations. For the sectioned FXT, most of the secondary stray light is suppressed by the inner mirror shells at angles of incidence shallower than the grazing angle. The nonreflection stray light appears at 1.5 times the grazing angle but only becomes significant above twice the grazing angle. Components of stray light overlap because the nested shells have different oblique angles.

In Fig. 7, we present the simulated images at discrete off-axis angles, 10′, 20′, 30′, and 40′. In the panel of the 40′ off-axis angle, the central square represents the FOV of an assumed detector. The weights of different types of rays are shown in Fig. 8, including normal light and the three remaining components of stray light, with an increasing off-axis angle. Compared to other components of stray light, the secondary stray light is not only brighter per unit area but also closer to the center of the detector. As a result, for the sectioned FXT, secondary stray light is the principal component of stray light to be suppressed by mounting an x-ray baffle. The x-ray baffle basically includes the sieve plate and the precollimator. For example, a sieve plate was employed for XMM-Newton[35] and a precollimator was utilized for eROSITA.[36] The x-ray baffle suppresses the stray light but simultaneously produces additional vignetting. By means of ray-tracing, the stray light problem and potential solutions will be analyzed, obtaining a trade-off between effective stray light reduction and vignetting avoidance.

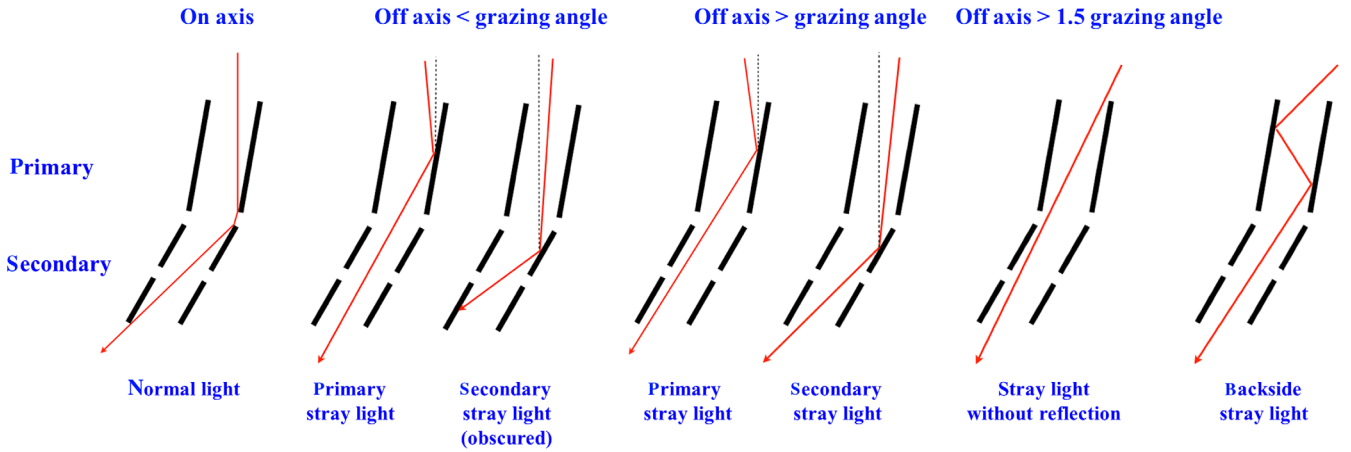

Fig. 6 Illustration of different behaviors of rays in the sectioned FXT.

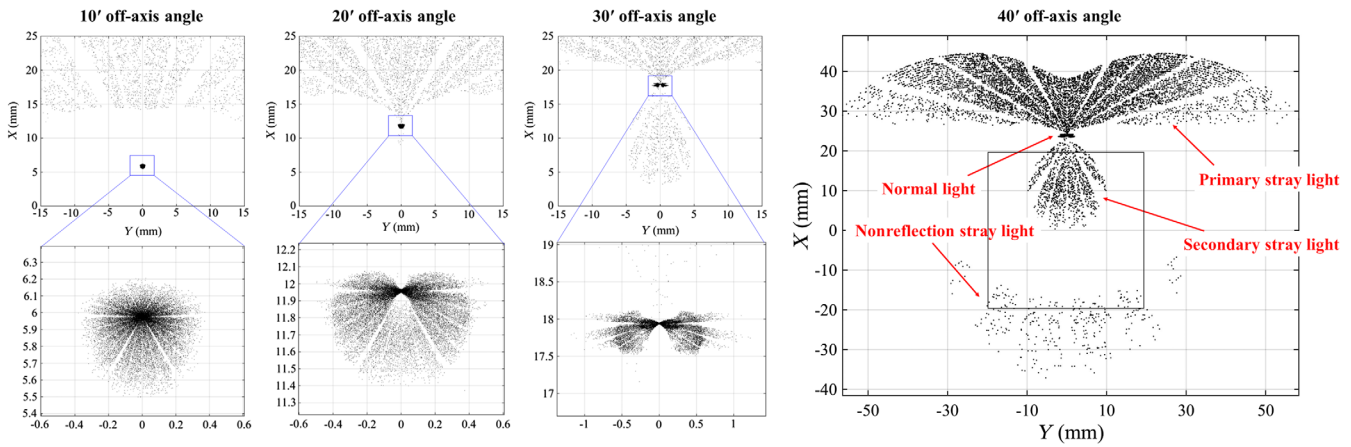

Fig. 7 Simulated images of the sectioned FXT at off-axis angles of 10′, 20′, 30′, and 40′.

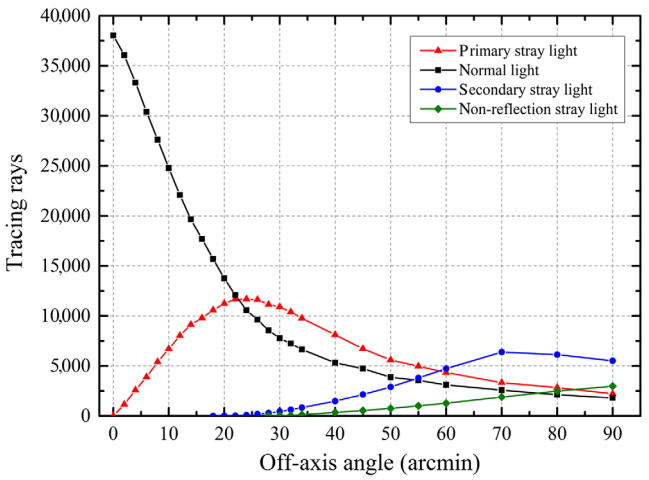

Fig. 8 Number of simulated rays of the various components in the sectioned FXT, in the case of 50,000 incoming parallel rays.

4 Hybrid Geometry

Comprising sectioned and nonsectioned geometries, the hybrid geometry is proposed as an alternative choice for x-ray telescopes with a large number of shells (Fig. 9). For the mirror shells with a small diameter (corresponding to shallow grazing angles), the oblique angles of the secondary mirror α and β after sectioning approach the oblique angle 3θ before sectioning (according to the inequality $\alpha < 3\theta < \beta$). Consequently, the difference in mirror oblique angles before and after sectioning is close to the fabrication accuracy. Thus, sectioning secondary mirrors are not only unnecessary but also difficult for the mirror shells with small diameters. Now that we can obtain a larger collecting area by nesting a large number of mirror shells, we can keep the inner mirror shells with small diameters unchanged but divide the secondary mirrors of the outer shells into two equal sections. Enlightened by the NuSTAR telescope, the intermediate shells between sectioned (outer shells) and nonsectioned shells (inner shells) could work as transition shells.[37,38] The transition shells are actually the outermost several shells of inner shells (the NuSTAR has three transition shells), which are nested with more graphited spacers. In addition, extra-wide outside spacers are utilized to bond the transition shells of adjacent sectors on single spacers, thus tying the optic together azimuthally. By means of the transition shells, the hybrid geometry will have better structural stability, albeit with a degradation in mounted figure and collecting area. The hybrid geometry is promising for obtaining both a large collecting area and decent angular resolution for conical Wolter-I geometry.

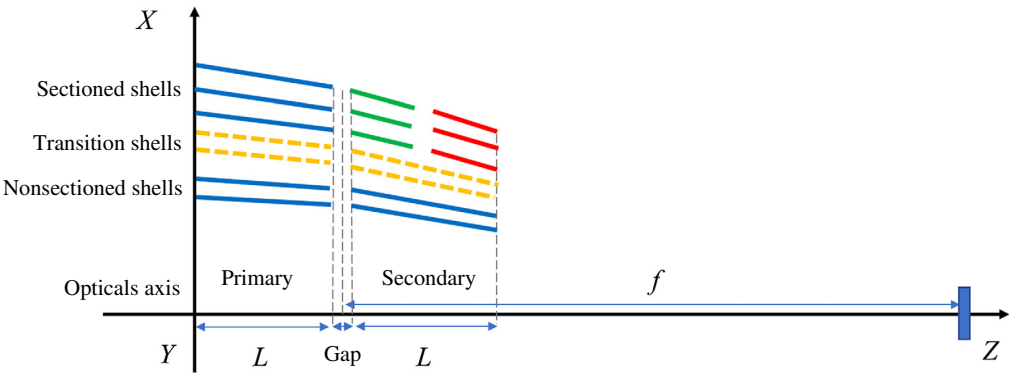

Fig. 9 Illustration of the hybrid geometry, which consists of sectioned shells (outer shells), transition shells (intermediate shells), and nonsectioned shells (inner shells).

5 Summary

We have described a procedure for modifying the parameters of conical Wolter-I geometry, to significantly improve its angular resolution. By dividing the secondary mirror into two sections along the optical axis, the conic error could be decreased by 50%, implying a 50% improvement in angular resolution (i.e., HPD). Furthermore, the sectioned geometry is characterized by a decent angular resolution over the whole FOV except for a good on-axis HPD. As a result, the geometric area will be reduced by only 5% because of the interval between the two sections, which can be improved by shortening the interval using improved fabrication process. Compared with sectioning secondary mirrors, shortening mirror length can also help improve the angular resolution but result in a significant reduction in effective area. Regarding our improvement in the thermal slumping technology, it is feasible to fabricate sectioned mirrors. In this paper, we introduced the equations for calculating parameters of the sectioned geometry. To confirm the improved performance, the behaviors of x-rays in the sectioned geometry and nonsectioned geometry were simulated. Apart from the HPD and effective area, we also studied the behaviors of stray light in the sectioned geometry by means of ray-tracing. The study of stray light allows us to design the x-ray baffle effectively in the next step, obtaining a trade-off between effective stray light reduction and vignetting avoidance. In addition, the hybrid geometry was presented as an alternative for x-ray telescopes with a large amount of nested shells, to obtain both a large collecting area and decent angular resolution for conical Wolter-I geometry.

Acknowledgments

We would like to express our gratitude to the anonymous reviewers for their fruitful comments to improve our article. This work was supported under the National Natural Science Foundation of China (Grant Nos. U1731242, 61621001, and 11427804), and the Fundamental Research Funds for the Central Universities.

References

1. V. H. Wolter, "Spiegelsysteme streifenden Einfalls als abbildende Optiken für Röntgenstrahlen," *Ann. Phys.* **445**(1–2), 94–114 (1952).
2. V. H. Wolter, "Verallgemeinerte Schwarzschildsche Spiegelsysteme streifender Reflexion als Optiken für Röntgenstrahlen," *Ann. Phys.* **445**, 286–295 (1952).
3. L. P. VanSpeybroeck and R. C. Chase, "Design parameters of paraboloid-hyperboloid telescopes for x-ray astronomy," *Appl. Opt.* **11**(2), 440–445 (1972).
4. W. Werner, "Imaging properties of Wolter I type x-ray telescopes," *Appl. Opt.* **16**(3), 764–773 (1977).
5. C. J. Burrows et al., "Optimal grazing incidence optics and its application to wide-field x-ray imaging," *Astrophys. J.* **392**(2), 760–765 (1992).
6. P. Conconi and S. Campana, "Optimization of grazing incidence mirrors and its application to surveying x-ray telescopes," *Astron. Astrophys.* **372**(3), 1088–1094 (2001).
7. P. L. Thompson and J. E. Harvey, "Development of an imaging performance criterion for wide-field grazing incidence x-ray telescopes," *Proc. SPIE* **3766**, 162–172 (1999).
8. J. E. Harvey et al., "Grazing-incidence hyperboloid-hyperboloid designs for wide-field x-ray imaging applications," *Appl. Opt.* **40**(1), 136–144 (2001).
9. T. T. Saha et al., "Optical design for a survey x-ray telescope," *Proc. SPIE* **9144**, 914418 (2014).
10. J. H. Underwood et al., "S056 x-ray telescope experiment on the Skylab Apollo Telescope Mount," *Appl. Opt.* **16**(4), 858–869 (1977).
11. R. Giacconi et al., "The Einstein /HEAO 2/ x-ray observatory," *Astrophys. J.* **230**, 540–550 (1979).
12. B. G. Taylor et al., "The EXOSAT mission," *Space Sci. Rev.* **30**, 479–494 (1981).
13. B. Aschenbach, "Design, construction, and performance of the ROSAT high-resolution x-ray mirror assembly," *Appl. Opt.* **27**(8), 1404–1413 (1988).
14. M. C. Weisskopf, "Chandra x-ray optics," *Opt. Eng.* **51**(1), 011013 (2012).
15. D. H. Lumb et al., "X-ray multi-mirror mission (XMM-Newton) observatory," *Opt. Eng.* **51**(1), 011009 (2012).
16. D. N. Burrows et al., "The swift, x-ray telescope," *Space Sci. Rev.* **120**(3–4), 165–195 (2005).
17. P. Friedrich et al., "Design and development of the eROSITA x-ray mirrors," *Proc. SPIE* **7011**, 70112T (2008).
18. S. Bowyer and R. F. Malina, "The extreme ultraviolet explorer mission," *Adv. Space Res.* **11**(11), 205–215 (1991).
19. P. L. Bornmann et al., "The GOES solar x-ray imager: overview and operational goals," *Proc. SPIE* **2812**, 309–319 (1996).
20. R. Petre and P. J. Serlemitsos, "Conical imaging mirrors for high-speed x-ray telescopes," *Appl. Opt.* **24**(12), 1833–1837 (1985).
21. P. J. Serlemitsos, "Conical foil x-ray mirrors: performance and projections," *Appl. Opt.* **27**(8), 1447–1452 (1988).
22. P. J. Serlemitsos et al., "The x-ray telescope on board ASCA," *Publ. Astron. Soc. Jpn.* **47**, 105–114 (1995).
23. L. Piro et al., "SAX: the wideband mission for x-ray astronomy," *Proc. SPIE* **2517**, 169–181 (1995).
24. P. J. Serlemitsos et al., "The x-ray telescope onboard Suzaku," *Publ. Astron. Soc. Jpn.* **59**, S9–S21 (2007).
25. K. K. Madsen et al., "The nuclear spectroscopic telescope array (NuSTAR) high-energy x-ray mission," *Astrophys. J.* **770**, 103 (2013).
26. T. Takahashi et al., "Hitomi (ASTRO-H) x-ray astronomy satellite," *J. Astron. Telesc. Instrum. Syst.* **4**(2), 021402 (2018).

27. S. E. Labov, "Figured grazing incidence mirrors from reheated float glass," *Appl. Opt.* **27**(8), 1465–1469 (1988).
28. S. Kraft et al., "Development of modular high-performance pore optics for the XEUS x-ray telescope," *Proc. SPIE* **5900**, 590010 (2005).
29. M. Beijersbergen et al., "Silicon pore optics: novel lightweight high-resolution x-ray optics developed for XEUS," *Proc. SPIE* **5488**, 868–874 (2004).
30. M. J. Collon et al., "Design, fabrication, and characterization of silicon pore optics for ATHENA/IXO," *Proc. SPIE* **8147**, 81470D (2011).
31. M. J. Collon et al., "Silicon pore optics for the ATHENA telescope," *Proc. SPIE* **9905**, 990528 (2016).
32. S. Chen et al., "Wolter-I-like x ray telescope structure using one conical mirror and one quadric mirror," *Chin. Opt. Lett.* **14**(12), 123401 (2016).
33. W. Yuan et al., "Einstein probe: a small mission to monitor and explore the dynamic x-ray universe," *Huazhong Univ. Sci. Tech. J.* **23**(4), 383 (2015).
34. Y. Liao et al., "Optical design and simulations of the soft x-ray telescope for Einstein Probe mission," *Proc. SPIE* **10399**, 103990L (2017).
35. D. Chambure et al., "The x-ray baffle of the XMM telescope: development and results," *Proc. SPIE* **3737**, 396–408 (1999).
36. P. Friedrich et al., "The eROSITA x-ray baffle," *Proc. SPIE* **9144**, 91444R (2014).
37. W. W. Craig et al., "Fabrication of the NuSTAR fight optics," *Proc. SPIE* **8147**, 81470H (2011).
38. J. E. Koglin et al., "First results from the ground calibration of the NuSTAR flight optics," *Proc. SPIE* **8147**, 81470J (2011).

Zhanshan Wang is a SPIE fellow and a professor at Tongji University. He received his MS degree in optics from Changchun Institute of Optics and Fine Mechanics, CAS, in 1988, and his PhD in optics from Shanghai Institute of Optics and Fine Mechanics, CAS, in 1996. He is the author of more than 150 journal papers. His current research interests include soft x-ray sources, optics in EUV and x-ray region, optical coatings for lasers and optical systems.

Biographies of the other authors are not available.